



# Ammonia Decomposition for Hydrogen Production in Catalytic Microchannels with Slip/Jump Effects

A. Qazi Zade<sup>1</sup>, M. Renksizbulut<sup>1†</sup> and J. Friedman<sup>2</sup>

<sup>1</sup>*Department of Mechanical and Mechatronics Engineering, University of Waterloo, Waterloo, ON, N2L 3G1, Canada*

<sup>2</sup>*Department of Mechanical and Industrial Engineering, Ryerson University, Toronto, ON, M5B 2K3, Canada*

†*Corresponding Author Email: metin@uwaterloo.ca*

(Received November 25, 2013; accepted August 19, 2014)

## ABSTRACT

The rarefaction effects on the catalytic decomposition of NH<sub>3</sub> in ruthenium-coated planar microchannels is numerically simulated in the Knudsen number range 0.015-0.03. A collocated finite-volume method is used to solve the governing equations. A concentration jump model derived from the kinetic theory of gases is employed to account for the concentration discontinuity at the reactive walls. A detailed surface reaction mechanism for ammonia decomposition on ruthenium along with a multi-component species diffusion model are used to study the effects of concentration jump coupled with velocity slip and temperature jump on the walls. The velocity-slip, temperature-jump and concentration-jump boundary conditions have miscellaneous effects on flow, temperature and species concentration fields. The results suggest that the velocity-slip boundary condition only slightly influences the species distribution at the edge of the Knudsen layer as well as inside the channel, while the temperature-jump boundary condition affects the heat and mass transfer characteristics the most. The concentration-jump effect, on the other hand, can counter balance the temperature-jump effects in some cases.

**Keywords:** Ammonia decomposition; Heterogeneous reactions; Velocity slip; Temperature jump; Concentration jump; Microchannel.

## NOMENCLATURE

$A_i$	pre-exponential factor	$t$	time
$c_{p,k}$	specific heat capacity	$T$	temperature
$D_{kj}$	tensor of ordinary diffusion coefficients	$T_s$	temperature of the gas at the edge of Knudsen layer
$D_k^T$	thermal diffusion coefficients	$u_s$	velocity of the gas at the edge of Knudsen layer
$E_i$	activation energy	$\mathbf{v}$	mass-averaged velocity vector
$h$	mixture enthalpy	$w_k$	molar mass of species $k$
$h_k$	enthalpy of species $k$	$\bar{w}$	mixture molar mass
$h_{f,k}^0$	standard enthalpy of formation	$X_k$	mole fraction of species $k$
$H$	channel height	$Y_k$	mass fraction of species $k$
$\mathbf{I}$	identity tensor	$Z_n$	site fraction of species $n$
$\mathbf{J}_k$	mass diffusion flux	$\bar{\gamma}$	specific heat ratio
$k_{ads,i}$	rate constant of reaction $i$	$\gamma_i$	sticking coefficient of adsorption reaction $i$
$L$	channel length	$\theta$	accommodation coefficient
$m$	reaction order	$\lambda$	thermal conductivity
$\vec{m}''$	mass flux	$\mu$	viscosity
$N_g$	total number of gas phase species	$\rho$	density
$N_s$	total number of surface species	$\sigma_n$	number of surface sites occupied by surface species $n$
$p$	pressure	$\Gamma$	surface site density
Pe	Peclet Number	$\Phi$	viscous dissipation
Re	Reynolds Number		
$R_k$	gas constant		
$\dot{s}_k$	production rate of gas phase species		
$\dot{s}_n$	production rate of surface species		

## 1. INTRODUCTION

In order to meet the increased power demand for micro-devices in almost every field of engineering, scaling down of conventional power supplies to micro-heat engines, micro fuel cells, micro-turbines and combustors has been proposed as an efficient, safe and reliable energy delivery method for Micro-Electro-Mechanical-Systems (MEMS). Due to high energy density of hydrocarbons compared to Lithium batteries and higher operational cycles, microburners have been studied in recent years as heat and energy sources for portable devices (Ahn *et al.* 2005, Fernandez-Pello 2002, Maruta 2011, Miesse and Masel 2004 and Yin *et al.* 2004). The energy is either utilized by thermoelectrics for electric power generation or through endothermic reactions such as fossil fuel steam reforming or ammonia decomposition for hydrogen production for fuel cells. The push towards reducing emission levels from hydrocarbon combustion has resulted in an interest in hydrogen production to power fuel cells. To avoid anode catalyst poisoning in Proton Exchange Membrane Fuel Cells (PEMFC), the hydrogen feed should be carbon monoxide free (less than 50 ppm). Conventional steam reforming and water gas-shift reactions could be employed to produce carbon-monoxide-free hydrogen from hydrocarbons in industrial scales. However, the process costs as well as transportation and storage costs make the on-site production of hydrogen an attractive option for hydrogen supply of fuel cells. Hydrogen production from a single step process such as ammonia decomposition is quite attractive especially in small-scale devices. Ammonia has been produced and stored in liquid form for a long time and issues about production, transportation, handling and storage are well established. Although even small traces (as low as 13 ppm) of ammonia can degrade PEM fuel cell performance, it is shown that the platinum catalyst of the fuel cell is not poisoned by ammonia; but rather the decrease in performance is because  $H^+$  ions are replaced by  $NH_4^+$  within the fuel cell anode catalyst layer (Uribe *et al.* 2002). Also, higher purity of available commercial ammonia makes it a better candidate for hydrogen production compared to methanol (Choudhary *et al.* 2001). Therefore, the availability, relatively easy decomposition with no need for added oxygen or steam and narrow explosion limits make ammonia a good candidate as a hydrogen carrier especially for portable devices. Scaling down the conventional reactors for hydrogen production is one approach. However, due to thermal and radical quenching at the walls, gas phase reactions are suppressed in gaps smaller than 1 ~ 2 millimeters (Fernandez-Pello 2002). Catalytic-wall reactors could also be employed to enhance reactions.

Microstructured reactors benefit from high process intensification, a wide reaction range up to explosion limits, reactor safety, faster process development and distributed production which make them suitable for highly endothermic and exothermic chemical reactions. As the push for

further miniaturization continues, modeling such systems becomes more and more complicated, since new physical phenomena should be taken into account. One of the complications in dealing with micro-scale devices is that the common continuum assumption can break down as the characteristic length scale of these devices approaches the mean molecular free path. In such a case, the number of inter-molecular collisions decreases and eventually there comes a stage in which the number of collisions between molecules are rare compared to the number of collisions with the surrounding walls, in which case each molecule acts independently to bring forth the gas properties (Kennard 1938). This makes the gas lose its intimate contact with solid bodies such that the gas “slips” over the surface, and in the case of heat or mass transfer, a temperature or concentration jump is observed between the surface and the adjacent gas layer. In the slip flow regime, the continuum equations can still be employed but proper velocity slip and temperature and concentration jump boundary conditions should be specified.

The effects of velocity slip and temperature jump on flow and heat transfer characteristics of non-reacting flows have been extensively studied in microchannels (Niazmand *et al.* 2010, Morini 2004, Renksizbulut *et al.* 2006, van Rij *et al.* 2009 and Yu and Ameen 2001). However, non-equilibrium transport in reacting flows still remains to be studied in-depth. In the case of multi-species transport, another important effect analogous to temperature jump should be taken into account, i.e., the concentration jump. There is very limited work on the concentration jump and its effects on catalytic reactions and the available literature has mainly focused on the temperature jump and velocity slip effects. The investigation of the concentration jump was initially performed by Kramers and Kistemaker (1943) based on the work of Maxwell on velocity slip and temperature jump. Concentration jump not only affects the rate of reaction and local species concentration, but also velocity slip and temperature jump in both reacting and non-reacting systems. Many rate-limiting adsorption/desorption reactions are very sensitive to local temperatures and hence the proper modeling and computation of temperature along with the local species concentration is vital for an accurate prediction of the behaviour of such systems. Therefore, all of these non-equilibrium effects should be considered simultaneously in the simulation of microreactors. This is even more pronounced in catalytic reactions since all the reactions take place on the wall. The effect of temperature jump on the performance of reactive systems was investigated and verified experimentally by Shankar and Glumac (2003) using low-pressure catalytic combustion systems. The concentration jump phenomenon has been detected in simulations of reacting gas mixtures by Bird (1994) and Papadopoulos and Rosner (1996). Xu and Ju (2005 and 2006) derived a concentration slip model and investigated the rarefaction effects on the rate of catalytic reactions in the numerical modeling of hydrogen and methane oxidation. In

their work, they considered the combustion of premixed stoichiometric mixtures at very low pressures ranging from 100 Pa to 0.2 atm. The velocity slip and temperature discontinuity at the wall were modeled using the conventional mixture-averaged boundary conditions. Li et al. (2008 and 2009) compared the effects of different operating conditions on the flame temperature of methane/air and hydrogen/air mixtures. They also studied the effects of first order velocity slip and temperature jump boundary conditions on the flame temperature. They reported negligible slip/jump effects at low velocities and large channels ( $d=1$  mm) and a considerable temperature discontinuity at the wall close to the flame region due to high radial gradients. More recently, Qazi Zadeet et al. (2012b) studied the non-equilibrium slip/jump effects in catalytic oxidation of lean hydrogen/air mixtures under different operating conditions. The presence of a temperature discontinuity at the wall was reported to be the main factor in defining the concentration jump at the edge of the Knudsen layer.

Small hydrogen generating devices have been developed and tested in recent years to meet the needs for on-site production of hydrogen for portable devices (Ganley 2004a, 2004b and Sørensen et al. 2005). Different catalysts and metal supports have been proposed and examined for hydrogen production. In these experiments the ammonia conversion rate has been measured for different geometries and operational conditions. The underlying detailed chemical kinetics of ammonia decomposition on different catalytic surfaces, however, is not well documented yet. Few studies have reported elementary reactions for ammonia decomposition and usually the global rate of reaction (one step) is presented for ammonia decomposition. Deshmukh et al. (2004) presented a detailed microkinetic model for describing surface chemistry of ammonia decomposition on ruthenium. Based on the microkinetic model, they used a reduced rate expression for numerical simulation of the experiment carried out by Ganley et al. (2004b). In the current research this set of elementary reactions will be used for numerical simulation of ammonia decomposition on ruthenium.

In the present work, the velocity slip, temperature jump and concentration jump effects on the catalytic decomposition of ammonia in planar microchannels are examined. To this end, the concentration jump, velocity slip and temperature jump boundary conditions derived by Qazi Zadeet et al. (2008) are employed. This set of boundary conditions, derived in their most general form, represent various terms in predicting the slip/jump conditions for reacting multicomponent mixtures. Unlike the first-order slip/jump boundary conditions where the mixture-averaged properties are utilized to relate the slip velocity and temperature discontinuity to the field variable gradients, this set of conditions accounts for individual species separately along with possible concentration discontinuity at the wall. Due to very small channel

sizes considered in the present study, the homogeneous reactions can be ignored as discussed in detail by QaziZadeet al. (2012a). Detailed surface reaction mechanisms are employed in order to fully account for the effects of surface species in determining the heterogeneous reaction pathways.

## 2. MATHEMATICAL MODEL

### 2.1 Governing Equations

A schematic view of channel geometry and the coordinate system are shown in Fig. 1. The channel height is  $H$  and the main flow is in the  $x$  direction. The governing mass, momentum, energy, and species continuity equations for a steady, laminar, reacting gas flow are:

$$\nabla \cdot (\rho \mathbf{V}) = 0 \quad (1)$$

$$\nabla \cdot (\rho \mathbf{V} \mathbf{V}) = -\nabla p + \nabla \cdot \left[ \mu (\nabla \mathbf{V} + \nabla \mathbf{V}^T) - \frac{2}{3} \mu (\nabla \cdot \mathbf{V}) \mathbf{I} \right] \quad (2)$$

$$\nabla \cdot (\rho \mathbf{V} h) = -\nabla \cdot (-\lambda \nabla T + \sum_{k=1}^{N_g} h_k \mathbf{J}_k) + \Phi \quad (3)$$

$$\nabla \cdot (\rho \mathbf{V} Y_k) = -\nabla \cdot \mathbf{J}_k \quad (4)$$

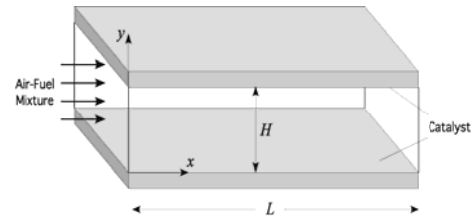


Fig. 1. Planar channel geometry and the coordinate system.

The molar production rate due to homogeneous reaction is excluded from the species continuity equation since homogeneous reaction effects can be neglected (Qazi Zade et al. 2012a). In this formulation, the enthalpy of the  $k^{th}$  species  $h_k$  and the mixture enthalpy  $h$  are defined as:

$$h_k = h_{f,k}^0 + \int_{T_0}^T c_{p,k} dT ; h = \sum_{k=1}^{N_g} h_k Y_k \quad (5)$$

In the present work, all effects due to thermal radiation and the Dufour effect are ignored. The species diffusion mass flux  $\mathbf{J}_k$  is determined using the multi-component diffusion equation as (Bird et al. 2001 and Hirschfelder et al. 1965):

$$\mathbf{J}_k = \frac{\rho w_k}{\bar{w}^2} \sum_{j=1}^{N_g} w_j D_{kj} \nabla X_j - D_k^T \frac{1}{T} \nabla T \quad (6)$$

The production rate of both gas and surface species on the wall are modeled using a detailed surface reaction mechanism proposed by Deshmukh et al. (2004) as shown in Table 1.

The forward reaction rate constants for this set of reactions are calculated as (Deshmukh et al. 2004):

$$k_{ads,i} = \frac{\gamma_i}{\Gamma^m} \sqrt{\frac{RT}{2\pi w_k}} \exp\left(\frac{-E_i}{RT}\right) \quad (7)$$

for adsorption

$$k_{f,i} = \frac{A_i}{\Gamma^{m-1}} \exp\left(\frac{-E_i}{RT}\right) \quad (8)$$

for desorption or surface reaction

**Table 1 Surface reaction mechanism of ammonia decomposition on ruthenium (Deshmukh et al. 2004); (s) denotes surface-adsorbed species; Arrhenius parameters for reaction rate constants:  $k_f = A\exp(-E_a/RT)$ .**

No.	Reaction	Sticking coefficient (unitless) or pre-exponential factor [ $\text{sec}^{-1}$ ]	$E_a$ [kcal/mol]
S1	$\text{H}_2 + 2\text{Ru(s)} \rightarrow 2\text{H(s)}$	$\gamma = 1.0$	1.9
S2	$2\text{H(s)} \rightarrow \text{H}_2 + 2\text{Ru(s)}$	$1.0 \times 10^{13}$	23.7
S3	$\text{N}_2 + 2\text{Ru(s)} \rightarrow 2\text{N(s)}$	$\gamma = 1.0$	14.1
S4	$2\text{N(s)} \rightarrow \text{N}_2 + 2\text{Ru(s)}$	$1.0 \times 10^{13}$	37.2
S5	$\text{NH(s)} + \text{Ru(s)} \rightarrow \text{N(s)} + \text{H(s)}$	$1.0 \times 10^{11}$	10.4
S6	$\text{N(s)} + \text{H(s)} \rightarrow \text{NH(s)} + \text{Ru(s)}$	$1.0 \times 10^{11}$	31.4
S7	$\text{NH}_2 + \text{Ru(s)} \rightarrow \text{NH(s)} + \text{H(s)}$	$1.0 \times 10^{11}$	19.1
S8	$\text{NH(s)} + \text{H(s)} \rightarrow \text{NH}_2 + \text{Ru(s)}$	$1.0 \times 10^{11}$	17.4
S9	$\text{NH}_3 + \text{Ru(s)} \rightarrow \text{NH}_2(\text{s}) + \text{H(s)}$	$1.0 \times 10^{11}$	17.5
S10	$\text{NH}_2(\text{s}) + \text{H(s)} \rightarrow \text{NH}_3 + \text{Ru(s)}$	$1.0 \times 10^{11}$	13.2
S11	$\text{NH}_3 + \text{Ru(s)} \rightarrow \text{NH}_3(\text{s})$	$\gamma = 1.0$	0
S12	$\text{NH}_3(\text{s}) \rightarrow \text{NH}_3 + \text{Ru(s)}$	$1.0 \times 10^{13}$	18.2

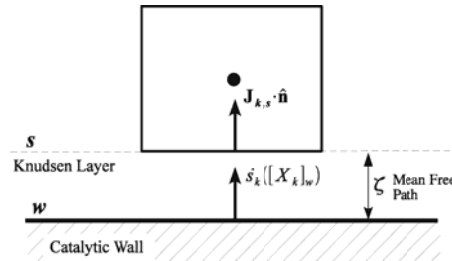


**Fig. 2. Schematic of a generic control volume next to the catalytic wall outside the Knudsen Layer.**

## 2.2 Boundary Conditions

Since a large number of variables can change in this type of problem, some parameters are kept constant in order to make a meaningful comparison between different cases. The inlet mass flux of each species, which is held constant, consists of the diffusion mass flux and the convective mass flux of that species. At low Peclet number flows, which is the case in the present work, the diffusive mass transfer generally becomes more effective. Since ammonia is consumed in the channel, right at the inlet there exists a positive diffusive mass flux of ammonia into the channel. In order to keep the total inlet mass flux constant, the inlet mass fraction of ammonia should be adjusted (lowered) accordingly. This way the total inlet mass flux of ammonia,  $\bar{m}''_{\text{NH}_3} = \rho Y_{\text{NH}_3} \mathbf{V} + \mathbf{J}_{\text{NH}_3}$  remains constant. On the other hand, the  $\text{H}_2$  produced in the channel can also diffuse back towards the inlet, which results in a negative diffusive mass flux of  $\text{H}_2$  out of the channel. Since the total mass flux of  $\text{H}_2$  (diffusion + convection) is set equal to zero in the simulations, this outgoing  $\text{H}_2$  mass flux should be balanced by the incoming convective flux of  $\text{H}_2$ , i.e.  $\rho Y_{\text{H}_2} \mathbf{V}$ , at the inlet. Therefore a finite amount of  $\text{H}_2$  will exist at the channel inlet, despite the fact that the inlet hydrogen mass flux is zero. At each iteration, the inlet mass fraction of all species  $Y_k$  and the mass-averaged inlet velocity  $\mathbf{V}$  are calculated using  $\bar{m}''_k = \rho Y_k \mathbf{V} + \mathbf{J}_k = \text{const}(N_g \text{ constraints})$  along

with  $\sum_{k=1}^{N_g} Y_k = 1$ . The diffusive fluxes of species  $\mathbf{J}_k$  are calculated from the previous iteration. This is discussed in more detail by Qazi Zade et al. (2012a).

The surface site density of the walls is specified to be  $\Gamma = 1.66 \times 10^{-5} \text{ mol/m}^2$  simulating a polycrystalline ruthenium coating (based on a ruthenium density of  $\rho_{\text{Ru}} = 12.45 \text{ g/cm}^3$ ) with a surface accommodation coefficient of 1.0. In the present work, the inlet gas temperature is assumed to be  $T_{\text{in}} = 300 \text{ K}$  while the wall temperature  $T_w$  is maintained at 1000 K, unless otherwise specified. The flow is mass driven such that the mass flux of each species is constant at the channel inlet. The outlet pressure is assumed to be atmospheric. In all simulations, a channel length of  $L = 20H$  is considered. However, due to the low ammonia decomposition rate, this channel length is not enough for complete ammonia consumption. Therefore, in order to handle the outlet boundary properly, the last 25% of the channel is assumed to be inert, allowing the flow, temperature and species fields to develop completely.

In the slip flow regime, the continuum equations for mass, momentum and energy conservation, described earlier, can still be employed but proper slip/jump boundary conditions should be specified to account for non-equilibrium effects in the Knudsen layer. The Knudsen layer is schematically depicted in Fig. 2 for a generic boundary cell. In the

case of multi-species transport, an important effect analogous to temperature-jump should be taken into account, i.e., the concentration-jump. In the present work, proper velocity slip, temperature jump and concentration jump boundary conditions, proposed by Qazi Zadeet al. (2008), are employed at the wall. In a reacting mixture, these boundary conditions can be expressed as:

$$\frac{(\rho Y_k)_w}{(\rho Y_k)_s} \left( \frac{T_w}{T_s} \right)^{\frac{1}{2}} (\theta_k - \gamma_k) = \theta_k \left( 1 + \frac{\tau_k^{yy}}{2p} \right)_s + (2 - \theta_k) \frac{J_{ky}}{\rho_{k,s}} \sqrt{\frac{\pi}{2R_k T_s}}$$

$$k = 1, \dots, N_g \quad (9)$$

$$u_s = \frac{\sum_{k=1}^{N_g} \frac{\rho_{k,s}}{\sqrt{w_k}} \left[ \theta_k \left( \frac{\lambda_k}{5\rho R} \frac{\partial \ln T}{\partial x} - \frac{J_{kx}}{\rho_k} \right) - (2 - \theta_k) \frac{\bar{w}_k^{xy}}{\rho_{k,s}} \sqrt{\frac{\pi}{2R_k T_s}} \right]}{\sum_{k=1}^{N_g} \frac{\rho_{k,s}}{\sqrt{w_k}} \left[ \theta_k \left( 1 + \frac{\tau_k^{yy}}{2p} \right) + (2 - \theta_k) \frac{J_{ky}}{\rho_k} \sqrt{\frac{\pi}{2R_k T_s}} \right]}$$

$$(10)$$

$$\frac{T_s}{T_w} = \frac{\sum_{k=1}^{N_g} \frac{\rho_k}{w_k^{3/2}} \left[ \frac{\bar{\gamma}+1}{4(\bar{\gamma}-1)} + \frac{u_s^2}{4R_k T_w} \right] \left[ \theta_k \left( 1 + \frac{\tau_k^{yy}}{2p} \right) + \frac{J_{ky}(2-\theta_k)}{\rho_k} \sqrt{\frac{\pi}{2R_k T_s}} \right]}{\sum_{k=1}^{N_g} \frac{\rho_k}{w_k^{3/2}} \left[ \frac{5(2-\theta_k)}{4} \sqrt{\frac{\pi}{2R_k T}} \left( \frac{J_{ky}}{\rho_k} - \frac{2\lambda_k}{5\rho R} \frac{\partial \ln T}{\partial y} \right) + \theta_k \mathfrak{S}_1 \right]}$$

$$(11)$$

where the Newtonian viscous stresses are defined as:

$$\tau_k^{xy} = -\mu_k \left( \frac{\partial U_x}{\partial y} + \frac{\partial U_y}{\partial x} \right) \quad (12a)$$

$$\tau_k^{yy} = \frac{2\mu_k}{3} \left( \frac{\partial U_x}{\partial x} + \frac{\partial U_z}{\partial z} - 2 \frac{\partial U_y}{\partial y} \right) \quad (12b)$$

$$\mathfrak{S}_1 = \frac{\bar{\gamma} + 1}{4(\bar{\gamma} - 1)} + \frac{\tau_k^{yy} (3\bar{\gamma} - 1)}{8p (\bar{\gamma} - 1)} + \frac{5 - 3\bar{\gamma}}{4(\bar{\gamma} - 1)} \frac{J_{ky}}{\rho_k} \sqrt{\frac{\pi}{2R_k T}}$$

$$(12c)$$

The accommodation coefficient  $\theta$  is equal to zero for specular reflection at the wall and equal to 1 for diffuse reflection (Chapman and Cowling 1970). This coefficient decreases for high temperatures and rough surfaces and typically can range between 0.1 to 1.0. In the present work, the surface accommodation coefficient is set equal to 1.0 for all species. In the derivation of Eq. (9), it is assumed that the velocity distribution of the molecules reflected from the surface does not depend on the species sticking coefficient or the local surface coverage of species.

In the absence of mass accumulation (e.g. etching or deposition) on an impermeable wall, the conservation of mass requires the diffusion mass flux of each gas phase species to be balanced by its production/destruction rate due to heterogeneous reactions  $\dot{s}_k$  on the wall as:

$$\dot{s}_k w_k = \mathbf{J}_k \cdot \hat{\mathbf{n}} \quad k = 1, 2, \dots, N_g \quad (13)$$

The rate of production/depletion of gas species  $\dot{s}_k$  depends on the molar concentration of species on the catalytic wall, not at the edge of the Knudsen layer. The relation between these values is dictated by the concentration jump boundary condition, i.e. Eq. (9).

On the other hand, the diffusion flux at the edge of the Knudsen layer into the gas-phase depends on the concentration gradients outside the Knudsen layer. This is shown schematically in Fig. 2 where a typical wall control volume is shown with respect to the Knudsen layer. The production rate of surface species  $\dot{s}_n$ , on the other hand, is governed by:

$$\frac{\partial Z_n}{\partial t} = \frac{\dot{s}_n}{\Gamma} \sigma_n - \frac{Z_n}{\Gamma} \frac{\partial \Gamma}{\partial t} \quad n = 1, 2, \dots, N_s \quad (14)$$

The second term on the right hand side of the above equation represents the change in the total number of available sites. In the present work, this term is dropped since due to the employed surface reaction mechanism scheme, the total number of available sites remains conserved as the reaction takes place on the walls. At steady state, the left hand side of this equation will also be zero which makes the net production rate of surface species  $\dot{s}_n$  equal to zero. However, the transient term in Eq. (14) is retained to facilitate the convergence of the system of equations (Mazumder and Lowry 2001). Surface species site fractions  $Z_n$ , by definition, should also satisfy the constraint  $\sum_{n=1}^{N_s} Z_n = 1$ .

Equations (12) and (13) form a set of stiff non-linear Differential Algebraic Equations (DAE) which is generally handled using the Newton method. The details about the numerical treatment of these equations are discussed by Coltrin *et al.* (1991) and Mazumder and Lowry (2001).

### 3. NUMERICAL IMPLEMENTATION

The formulation presented in Eqs. (1-4) is an elliptic model where the axial diffusion terms are retained. These equations were discretized using the finite volume method. A non-staggered (colocated) arrangement was employed for the solution of the flow field following the Rhie and Chow (1983) formulation. Implementing the Pressure Weighted Interpolation Method (PWIM), the control volume face velocities are related to nodal pressure values. A deferred correction scheme is also used to improve the upwind approximation in discretizing the advection terms. After each step in the solution of gas phase species, the flux matching boundary condition (13) and the surface species production rate (14) equations are solved on every wall element. The connection between the molar concentration of species on the wall and at the edge of the Knudsen layer is established utilizing the concentration jump boundary condition. In each iteration, the molar concentration of species at the wall required for the calculation of the heterogeneous production rate  $\dot{s}_k$  in Eq. (13) are written in terms of the molar concentration of species at the edge of the Knudsen layer using Eq. (9). This way, Eqs. (13) and (14) will form a closed set of  $N_g + N_s$  equations to solve for the molar concentration of species at the edge of the Knudsen layer and surface coverage of species at the wall. This set of non-linear DAEs are solved using the SUNDIALS code (Hindmarsh *et al.* 2005).

The solution to this set of equations yields the

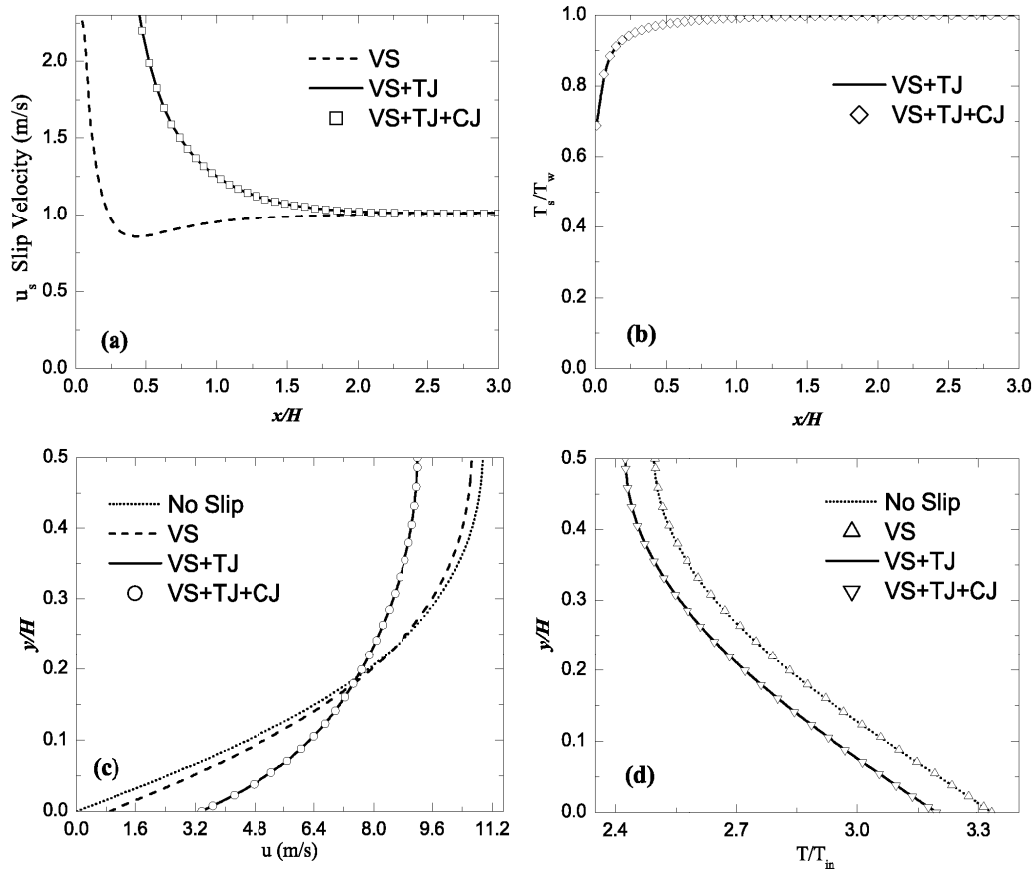


**Fig. 3. Velocity slip (a) and temperature jump (b) at the edge of the Knudsen layer along a  $H = 15 \mu\text{m}$  channel with an inlet mass flux of  $\bar{m}_{in}'' = 2 \text{ kg/m}^2\text{s}$  under different slip/jump boundary conditions. Streamwise velocity (c) and temperature (d) distributions at  $x/H = 0.33$ .**

surface species site fractions on the *wall* and the mass fractions of gas phase species at the edge of the *Knudsen layer* which are employed as the proper boundary conditions for the next iteration. The mixture transport properties as well as the pure species properties are obtained using the CHEMKIN database (Kee et al. 1986). The solution domain is discretized using an orthogonal non-uniform grid distribution. Grid point density is higher near the wall and channel inlet since the highest gradients are expected in these regions. Different mesh sizes were examined in order to test the grid independence of the results. A mesh size of  $140 \times 24$  (with an expansion ratio of 1.02 and 1.025 in the  $x$  and  $y$  directions, respectively) yields grid-independent results. Also, since the channel geometry and boundary conditions are symmetric, only half of the channel is simulated numerically.

The numerical code is validated at different stages. Initially, a 3D extension of the code is developed for non-reacting compressible flow of air within rectangular channels. Grid independence and validation against the available theoretical and numerical predictions are presented in Qazi Zade et al. (2011). The gas phase and catalytic reactions are validated afterwards by comparing the simulation results with the experimental and numerical data of Appel et al. (2002) in a planar geometry. Streamwise and cross-sectional species mass fraction distributions as well as the temperature field in the

channel were all in good agreement with available experimental and numerical data (Qazi Zade et al. 2012a and 2012b). Finally, the proposed set of boundary conditions for multicomponent mixtures given in section 2.2 are validated against the predictions of Direct Simulation Monte Carlo (DSMC) method for non-reacting  $\text{H}_2/\text{N}_2$  and  $\text{H}_2/\text{N}_2/\text{CO}_2$  mixtures as presented in Qazi Zade et al. (2012c).

#### 4. RESULTS AND DISCUSSION

In this section, the effects of slip/jump boundary conditions on various field variables are discussed. The previously described velocity slip, temperature jump and concentration jump boundary conditions are denoted by “VS”, “TJ” and “CJ”, respectively. Pure ammonia enters the channel with an inlet mass flux of  $\bar{m}_{in}'' = 2 \text{ kg/m}^2\text{s}$  while the temperature at the walls are kept constant  $T_w = 1000 \text{ K}$ . Two channel sizes of  $H = 15 \mu\text{m}$  and  $H = 30 \mu\text{m}$  are considered here. The range of Knudsen number encountered in this work is 0.015-0.03 (based on channel height and hydrogen mean free path).

Velocity and temperature distributions across the channel as well as velocity slip and temperature jump along a  $H = 15 \mu\text{m}$  channel are shown in Fig. 3 (a) and (b) under different boundary condition combinations. When only the velocity slip boundary condition is considered, the temperature at the edge

of the Knudsen layer is equal to the wall temperature, which eliminates the axial temperature gradient. In such a case, the wall shear stress  $\tau^{xy}$  governs the slip velocity behavior. Due to the very low Reynolds number ( $Re \sim 1$ ), normal velocity gradients are only significant close to the channel inlet and quickly fade out further down the channel. Therefore, except for regions close to the inlet, the velocity slip does not influence the flow field to a great extent. On the other hand, the temperature discontinuity at the wall significantly affects the slip velocity. The presence of a strong temperature gradient along the wall in the developing region of the channel increases the slip velocity. The temperature jump itself is mostly influenced by the temperature gradient normal to the wall. Again, the highly diffusive nature of the transport processes in these small channels ( $Pe \sim 1$ ) diminishes the gradients within about one channel height into the channel.

The concentration jump boundary condition, however, does not alter the velocity slip and temperature jump at the wall and its influence is negligible. Although, as will be discussed later, the species mass fractions are affected by the concentration jump boundary condition, their effect on the mixture properties is minimal and hence does not influence the flow and temperature fields. The above-mentioned effects are more evident in Fig. 3 (c) and (d) where the velocity and temperature fields are sketched across the channel at  $x/H = 0.33$  under different boundary condition combinations. Clearly, in this operating condition, the presence of temperature jump is the most important factor in defining both the velocity and temperature fields. The minimal effect of concentration jump boundary condition on the velocity and temperature distributions across the channel is also evident.

Due to the constant mass flux boundary condition imposed at the inlet, the species mass fractions can be different under different wall boundary condition combinations. The inlet mass fractions of  $NH_3$  and  $H_2$  are shown in Fig. 4 for a  $H = 15 \mu m$  channel under different types of wall boundary condition combinations. Right at the channel inlet, due to ammonia consumption in the channel, there exists a positive diffusive mass flux of  $NH_3$  into the channel. In order to keep the total ammonia inlet mass flux constant, the inlet mass fraction of ammonia should be adjusted (lowered) accordingly. On the other hand, the hydrogen and nitrogen produced in the channel can diffuse back towards the channel inlet which results in a negative diffusive mass flux of  $H_2$  and  $N_2$  out of the channel. Since the total mass flux (diffusion + convection) of the reaction products is set equal to zero in the simulations, the outgoing diffusive mass flux of  $H_2$  and  $N_2$  should be balanced by the incoming convective flux, i.e.  $\rho Y_{H_2} \mathbf{V}$  and  $\rho Y_{N_2} \mathbf{V}$ , at the inlet. Therefore a finite amount of  $H_2$  and  $N_2$  will exist at the channel inlet despite their zero total inlet mass flux. It is evident that the velocity slip boundary condition alone does not affect the inlet composition. However, the presence of a

temperature discontinuity noticeably alters the inlet hydrogen mass fraction especially in regions close to the wall.

The species mass fractions of  $H_2$ ,  $N_2$  and  $NH_3$  at the edge of the Knudsen layer are shown in Fig. 5 for a  $H = 15 \mu m$  channel.

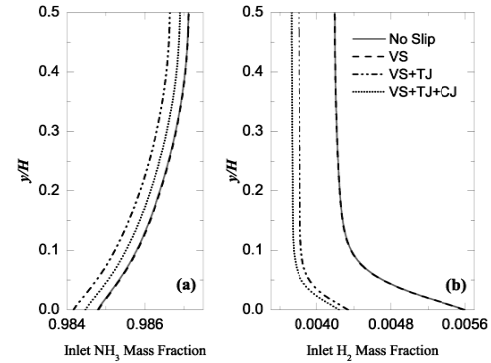


**Fig. 4. Inlet  $NH_3$  and  $H_2$  mass fractions for different types of wall boundary conditions.**

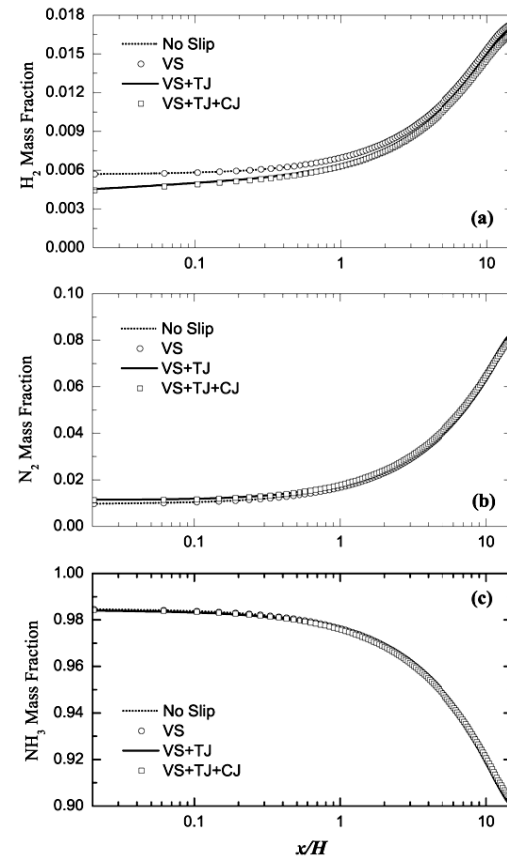


**Fig. 5.  $H_2$  (a),  $N_2$  (b) and  $NH_3$  (c) mass fractions at the edge of the Knudsen layer under different types of wall boundary conditions along the channel.**

As observed, the velocity slip influence on the species mass fractions is minimal. It is due to the fact that the presence of velocity slip alone at the wall does not significantly change the velocity and temperature fields (Qazi Zade *et al.* 2012b). The decrease in the hydrogen mass fraction in the “VS+TJ” cases is mainly due to the decreased

hydrogen levels at the inlet. The presence of strong axial temperature gradient as a result of “TJ” significantly increases the velocity slip at the edge of the Knudsen layer. The increased slip velocity close to the wall decreases the inlet hydrogen mass fraction in this region as observed in Fig 4. In addition, the increased near-wall velocity alters the velocity and temperature distributions in the channel. The nitrogen and ammonia mass fractions at the edge of the Knudsen layer remain intact with the introduction of slip/jump boundary conditions.

In order to investigate slip/jump effects on species transport, the catalytic production rates of  $H_2$  under various boundary condition combinations are shown in Fig. 6. Due to a very low Reynolds number, the transport of species and energy is generally diffusive, and therefore, the velocity slip does not alter the mass and energy transfer significantly. As such, the velocity slip boundary condition alone has a very small impact on the hydrogen production rate. However, the influence of the temperature jump boundary condition is noticeable, especially in the developing region of the  $H = 15 \mu m$  channel. The increase in the catalytic hydrogen production due to the presence of temperature discontinuity diminishes as the channel size increases, as observed in Fig. 6 (b). This is in accord with the decreased Knudsen number (curtailing slip/jump effects in general) in the larger channel.

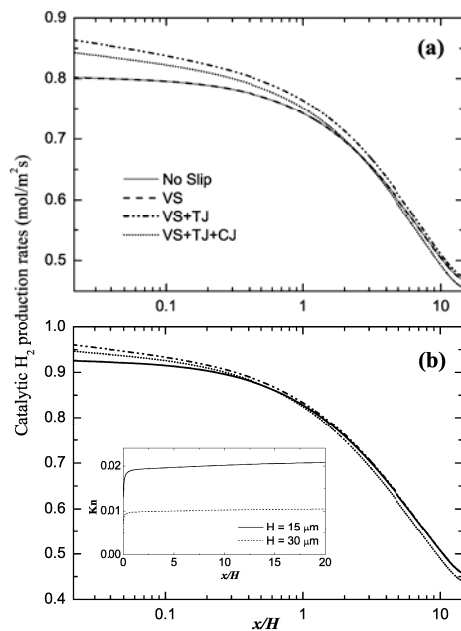


**Fig. 6. Catalytic production rates of  $H_2$  along the channel for (a)  $H = 15 \mu m$  and (b)  $H = 30 \mu m$  under different types of boundary condition combinations.**

The axial temperature gradient at the edge of the Knudsen layer substantially increases the slip velocity, which in turn enhances the convective mass transfer and causes steeper gradients in the vicinity of the wall. As can be inferred from Eq. (12) steeper normal gradients (higher diffusion mass flux) increase the species reaction rates  $s_k$ . As

the temperature jump boundary condition is introduced, the conversion rate experiences a considerable increase in the developing region and then merges with the no-slip case result further downstream. The presence of concentration discontinuity at the wall, on the other hand, counter balances the increase in hydrogen production rate by reducing the species mass fraction gradient normal to the wall. The decrease in the concentration gradients (and consequently the ammonia diffusive mass flux towards the wall) translates into lower hydrogen production rates as can be readily seen in Eq. (12). Lower hydrogen level at the inlet in the presence of temperature discontinuity at the wall also contributes to higher levels of hydrogen production in the case of “TJ”.

Species coverage on the catalytic wall is also influenced by the slip/jump boundary conditions. Figure 7 shows the surface coverage  $Z_k$  of different species at the wall for a  $H = 15 \mu m$  channel. Close to the channel inlet, the surface is dominated by free sites and  $N(s)$ . As ammonia reacts along the channel, the increased hydrogen in the channel gives rise to  $H(s)$  coverage. Although the nitrogen level in the channel is also increased, the adsorbed hydrogen coverage starts increasing at the expense of  $N(s)$  due to the much lower activation energy barrier (see Table 1). As with other variables before, the velocity slip alone does not influence the surface species coverages. In the presence of temperature jump the change in  $H(s)$  and  $N(s)$  coverages compared to the “No Slip” case follows the same trend as the mass fractions of  $H_2$  and  $N_2$  at the edge of the Knudsen layer; i.e. slightly lower  $H(s)$  and slightly higher  $N(s)$  coverages. The available free sites  $Ru(s)$  and  $NH_3(s)$  are influenced the most by the presence of concentration discontinuity at the wall.

### 3. CONCLUSIONS

In this paper, non-equilibrium slip/jump effects in catalytic ammonia decomposition on ruthenium are numerically studied in planar microchannels. A colocated finite volume method is used to solve the transport equations with surface reactions under different operating conditions. A complete set of slip/jump boundary conditions derived from the kinetic theory of gases is used along with continuum equations to account for rarefaction effects. Besides the velocity slip and temperature discontinuity at the wall, the effects of concentration jump are also investigated.

The concentration jump effect on the flow and temperature fields is found to be negligible since the mass-averaged properties of the mixture do not vary considerably. In the range of operating conditions considered in the present work, the temperature jump boundary condition affects the

flow and temperature fields the most. The presence of strong axial temperature gradients at the channel inlet substantially increases the velocity. The velocity slip boundary condition only slightly influences the species distribution at the edge of the Knudsen layer as well as inside the channel.

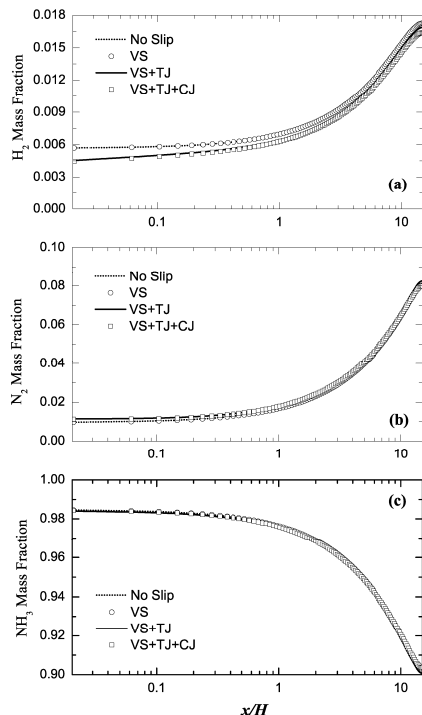


**Fig. 7. Surface species coverage of Ru(s), H(s), N(s) and NH<sub>3</sub>(s) for a  $H = 15 \mu\text{m}$  channel at the wall under different types of wall boundary conditions along the channel.**

Numerical results show that the presence of temperature discontinuity at the wall increases ammonia decomposition and as the channel size decreases, this effect becomes more evident. The presence of concentration discontinuity at the wall, on the other hand, counter balances the increase in hydrogen production rate by reducing the species mass fraction gradient normal to the wall. As the temperature jump boundary condition is introduced, the hydrogen mass fraction at the edge of the Knudsen layer decreases mainly due to the decreased hydrogen levels at the inlet. With the rise in hydrogen level within the channel due to ammonia decomposition, the H(s) surface coverage increases along the channel as well. However, since hydrogen adsorption has a much lower activation energy barrier, the adsorbed hydrogen coverage starts increasing at the expense of N(s) despite the fact that nitrogen is also being produced in the process.

#### ACKNOWLEDGEMENTS

The support of the Ontario Graduate Scholarship to Azad Qazi Zade is gratefully acknowledged.

#### REFERENCES

Ahn, J., C. Eastwood, L. Sitzki and P. D. Ronney (2005). Gas- phase and catalytic combustion in heat-recirculating burners. *Proc. Combust. Inst.* 30, 2463-2472.

Appel, C., J. Mantzaras, R. Schaeren, R. Bombach, A. Inauen, B. Kaeppli, B. Hemmerling and A.

Stampanoni (2002). An experimental and numerical investigation of homogeneous ignition in catalytically stabilized combustion of hydrogen/air mixtures over platinum. *Combust. Flame* 128(4), 340-368.

Bird, G. A. (1994). *Molecular Gas Dynamics and the Direct Simulation of Gas Flows*. New York: Oxford University Press.

Bird, R. B., W. E. Stewart and E. N. Lightfoot (2001). *Transport Phenomena* (2<sup>nd</sup> ed.). New York: John Wiley & Sons.

Chapman, S. and T. G. Cowling (1970). *The Mathematical Theory of Non-Uniform Gases* (3<sup>rd</sup> ed.). London: Cambridge University Press.

Choudhary, T. V., C. Sivadinarayana and D. Goodman (2001). Catalytic ammonia decomposition: CO<sub>x</sub>-free hydrogen production for fuel cell applications. *Catal. Lett.* 72(3-4), 197-201.

Coltrin, M. E., R. J. Kee and F. M. Rupley (1991). Surface Chemkin: A general formalism and software for analyzing heterogeneous chemical kinetics at gas-solid interfaces. *Int. J. Chem. Kinet.* 23(12), 1111-1128.

Deshmukh, S. R., A. B. Mhadeshwar and D. G. Vlachos (2004). Microreactor modeling for hydrogen production from ammonia decomposition on ruthenium. *Ind. Eng. Chem. Res.* 43, 2986-2999.

Fernandez-Pello, A. C. (2002). Micropower generation using combustion: Issues and approaches. *Proc. Combust. Inst.* 29, 883- 899.

Ganley, J. C., E. G. Seebauer and R. I. Masel (2004a). Development of a microreactor for the production of hydrogen from ammonia. *J. Power Sources* 137(1), 53-61.

Ganley, J. C., E. G. Seebauer and R. I. Masel (2004b). Porous anodic alumina microreactors for production of hydrogen from ammonia. *AIChE J.* 50(4), 829-834.

Hindmarsh, A. C., P. N. Brown, K. E. Grant, S. L. Lee, R. Serban, D. E. Shumaker and C. S. Woodward (2005). SUNDIALS: Suite of nonlinear and differential/algebraic equation solvers. *ACM Transactions on Mathematical Software* 31(3), 363-396.

Hirschfelder, J. O., C. F. Curtiss and R. B. Bird (1965). *Molecular Theory of Gases and Liquids* (2<sup>nd</sup> ed.). New York: John Wiley & Sons.

Kee, R. J., G. Dixon Lewis, J. Warnatz, M. E. Coltrin and J. A. Miller (1986). A fortran computer package for the evaluation of gas-phase multicomponent transport properties. Technical Report SAND87-8246, Sandia.

- Kennard, E. H. (1938). *Kinetic Theory of Gases*. New York: McGraw-Hill.
- Kramers, H. A. and J. Kistemaker (1943). On the slip of a diffusing gas mixture along a wall. *Physica X* 8, 699-713.
- Li, J., S. K. Choua, Z. W. Li and W. M. Yang (2008). A comparative study of H<sub>2</sub>-air premixed flame in micro combustors with different physical and boundary conditions. *Combust. Theor. Model.* 12(2), 325-347.
- Li, J., S. K. Choua, W. M. Yanga and Z. W. Li (2009). A numerical study on premixed micro-combustion of CH<sub>4</sub>-air mixture: Effects of combustor size, geometry and boundary conditions on flame temperature. *Chem. Eng. J.* 150, 213-222.
- Maruta, K. (2011). Micro and mesoscale combustion. *Proc. Combust. Inst.* 33, 125-150.
- Mazumder, S. and S. A. Lowry (2001). The treatment of reacting surfaces for finite-volume schemes on unstructured meshes. *J. Comput. Phys.* 173(2), 512-526.
- Miesse, C. M. and R. I. Masel (2004). Submillimeter-scale combustion. *AIChE J.* 50(12), 3206-3214.
- Morini, G. L. (2004). Single-phase convective heat transfer in microchannels: a review of experimental results. *Int. J. Therm. Sci.* 43(7), 631-651.
- Niazmand, H., A. A. Jagharghand and M. Renksizbulut (2010). Slip-flow and heat transfer in isoflux rectangular microchannels with thermal creep effects. *Journal of Applied Fluid Mechanics* 3, 33-41.
- Papadopoulos, D. H. and D. E. Rosner (1996). Direct simulation of concentration creep in a binary gas-filled enclosure. *Phys. Fluids* 8, 3179-3193.
- Qazi Zade, A., M. Renksizbulut and J. Friedman (2008). Slip/jump boundary conditions for rarefied reacting/non-reacting multi-component gaseous flows. *Int. J. Heat Mass Transfer* 51(21-22), 5063-5071.
- Qazi Zade, A., M. Renksizbulut and J. Friedman (2011). Heat transfer characteristics of developing gaseous slip-flow in rectangular microchannels with variable physical properties. *Int. J. Heat and Fluid Flow* 32, 117-127.
- Qazi Zade, A., M. Renksizbulut and J. Friedman (2012a). Contribution of homogeneous reactions to hydrogen oxidation in catalytic microchannels. *Combust. Flame* 159(2), 784-792.
- Qazi Zade, A., M. Renksizbulut and J. Friedman (2012b). Rarefaction effects on the catalytic oxidation of hydrogen in microchannels. *Chem. Eng. J.* (181-182), 643-654.
- Qazi Zade, A., A. Ahmadzadegan and M. Renksizbulut (2012c). A detailed comparison between Navier-Stokes and DSMC simulations of multicomponent gaseous flow in microchannels. *Int. J. Heat Mass Transfer* 55, 4673-4681.
- Renksizbulut, M., H. Niazmand and G. Tercan (2006). Slip-flow and heat transfer in rectangular microchannels with constant wall temperature. *Int. J. Therm. Sci.* 45(9), 870-881.
- Rhie, M. C. and W. L. Chow (1983). Numerical study of the turbulent flow past an airfoil with trailing edge separation. *AIAA J.* 21(11), 1525-1532.
- Shankar, N. and N. Glumac (2003). Experiment alinvestigations into the effect of temperature slip on catalytic combustion. *Eastern States Section Meeting of the Combustion Institute*. Penn State University.
- Sorensen, R. Z., L. J. E. Nielsen, S. Jensen, O. Hansen, T. Johannessen, U. Quaade and C. H. Christensen (2005). Catalytic ammonia decomposition: miniaturized production of CO<sub>x</sub>-free hydrogen for fuel cells. *Catal. Commun.* 6, 229-232.
- Uribe, F. A., S. Gottesfeld and T. A. Zawodzinski (2002). Effect of ammonia as potential fuel impurity on proton exchange membrane fuel cell performance. *J. Electrochem. Soc.* 149(3), A293- A296.
- Van Rij, J., T. A. Ameel and T. Harman (2009). An evaluation of secondary effects on microchannel frictional and convective heat transfer characteristics. *Int. J. Heat Mass Transfer* 52(11-12), 2792-2801.
- Xu, B. and Y. Ju (2005). Concentration slip and its impact on heterogeneous combustion in a micro-scale chemical reactor. *Chem. Eng. Sci.* 60, 3561-3572.
- Xu, B. and Y. Ju (2006). Theoretical and numerical studies of non-equilibrium slip effects on a catalytic surface. *Combust. Theor. Model* 10(6), 961-979.
- Yin, S. F., B. Q. Xu, X. P. Zhou and C. T. Au (2004). A mini-review on ammonia decomposition catalysts for on-site generation of hydrogen for fuel cell applications. *Appl. Catal. A* 277, 1-9.
- Yu, S. and T. A. Ameel (2001). Slip flow heat transfer in rectangular microchannels. *Int. J. Heat Mass Transfer* 44(22), 4225- 4234.